



Inglis, G. N., Collinson, M., Riegel, W., Wilde, V., Farnsworth, A., Lunt, D., ... Pancost, R. (2017). Mid-latitude continental temperatures through the early Eocene in western Europe. *Earth and Planetary Science Letters*, 460, 86-96.

Publisher's PDF, also known as Version of record

License (if available):  
CC BY-NC-ND

[Link to publication record in Explore Bristol Research](#)  
PDF-document

This is the final published version of the article (version of record). It first appeared online via Elsevier at DOI: 10.1016/j.epsl.2016.12.009. Please refer to any applicable terms of use of the publisher.

## University of Bristol - Explore Bristol Research

### General rights

This document is made available in accordance with publisher policies. Please cite only the published version using the reference above. Full terms of use are available:  
<http://www.bristol.ac.uk/pure/about/ebr-terms.html>



## Mid-latitude continental temperatures through the early Eocene in western Europe



Gordon N. Inglis<sup>a,b,\*</sup>, Margaret E. Collinson<sup>c</sup>, Walter Riegel<sup>d</sup>, Volker Wilde<sup>d</sup>, Alexander Farnsworth<sup>b,e</sup>, Daniel J. Lunt<sup>e,b</sup>, Paul Valdes<sup>e</sup>, Brittany E. Robson<sup>c</sup>, Andrew C. Scott<sup>c</sup>, Olaf K. Lenz<sup>f</sup>, B. David A. Naafs<sup>a,b</sup>, Richard D. Pancost<sup>a,b</sup>

<sup>a</sup> Organic Geochemistry Unit, School of Chemistry, University of Bristol, Cantock's Close, Bristol BS8 1TS, UK

<sup>b</sup> Cabot Institute, University of Bristol, Bristol, BS8 1UJ, UK

<sup>c</sup> Department of Earth Sciences, Royal Holloway University of London, Egham, Surrey TW20 0EX, UK

<sup>d</sup> Senckenberg Forschungsinstitut und Naturmuseum, Senckenberganlage 25, D-60325 Frankfurt am Main, Germany

<sup>e</sup> BRIDGE, School of Geographical Sciences, University of Bristol, University Road, Bristol BS8 1SS, UK

<sup>f</sup> TU Darmstadt, Institut für Angewandte Geowissenschaften, Angewandte Sedimentgeologie, Schnittspahnstrasse 9, 64287 Darmstadt, Germany

### ARTICLE INFO

#### Article history:

Received 11 January 2016

Received in revised form 30 November 2016

Accepted 7 December 2016

Available online 22 December 2016

Editor: H. Stoll

#### Keywords:

early Palaeogene  
terrestrial temperature  
GDGTs  
lignite  
coal  
greenhouse climates

### ABSTRACT

Branched glycerol dialkyl glycerol tetraethers (brGDGTs) are increasingly used to reconstruct mean annual air temperature (MAAT) during the early Paleogene. However, the application of this proxy in coal deposits is limited and brGDGTs have only been detected in immature coals (i.e. lignites). Using samples recovered from Schöningen, Germany (~48°N palaeolatitude), we provide the first detailed study into the occurrence and distribution of brGDGTs through a sequence of early Eocene lignites and associated interbeds. BrGDGTs are abundant and present in every sample. In comparison to modern studies, changes in vegetation type do not appear to significantly impact brGDGT distributions; however, there are subtle differences between lignites – representing peat-forming environments – and siliciclastic nearshore marine interbed depositional environments. Using the most recent brGDGT temperature calibration (MAT<sub>mr</sub>) developed for soils, we generate the first continental temperature record from central-western continental Europe through the early Eocene. Lignite-derived MAAT estimates range from 23 to 26 °C while those derived from the nearshore marine interbeds exceed 20 °C. These estimates are consistent with other mid-latitude environments and model simulations, indicating enhanced mid-latitude, early Eocene warmth. In the basal part of the section studied, warming is recorded in both the lignites (~2 °C) and nearshore marine interbeds (~2–3 °C). This culminates in a long-term temperature maximum, likely including the Early Eocene Climatic Optimum (EECO). Although this long-term warming trend is relatively well established in the marine realm, it has rarely been shown in terrestrial settings. Using a suite of model simulations we show that the magnitude of warming at Schöningen is broadly consistent with a doubling of CO<sub>2</sub>, in agreement with late Paleocene and early Eocene *p*CO<sub>2</sub> estimates.

© 2016 The Author(s). Published by Elsevier B.V. This is an open access article under the CC BY-NC-ND license (<http://creativecommons.org/licenses/by-nc-nd/4.0/>).

### 1. Introduction

Gradual surface ocean warming during the late Paleocene and early Eocene (Hollis et al., 2012; Frieling et al., 2014) culminated in the Early Eocene Climatic Optimum (EECO; 53–51 Ma), a long-term global temperature maximum associated with high atmospheric carbon dioxide concentrations (*p*CO<sub>2</sub>) (Anagnostou et al., 2016) and the absence of large continental ice sheets (Zachos et al., 2001). During the EECO, TEX<sub>86</sub>-based mid-to-high latitude sea

surface temperature (SST) estimates exceed 25 °C, resulting in a reduced latitudinal SST gradient (Hollis et al., 2012; Bijl et al., 2013; Frieling et al., 2014; Inglis et al., 2015b). However, these climate conditions have proven difficult to reconcile with modelling simulations (Lunt et al., 2012), although recent progress has been made (Sagoo et al., 2013). As the terrestrial heat budget is more easily characterised in model simulations than the ocean heat budget (Huber and Caballero, 2011), workers have cited the need for additional terrestrial temperature records spanning the early Eocene (e.g. Huber and Caballero, 2011).

Palaeobotanical techniques, such as CLAMP (Climate-Leaf Analysis Multivariate Program), LMA (Leaf Margin Analysis) and CA (Coexistence Approach), have previously shown that mid-to-high lati-

\* Corresponding author at: Organic Geochemistry Unit, School of Chemistry, University of Bristol, Cantock's Close, Bristol BS8 1TS, UK.

E-mail address: [gordon.inglis@bristol.ac.uk](mailto:gordon.inglis@bristol.ac.uk) (G.N. Inglis).

tude mean annual temperature estimates (MAT) were warmer than modern during the early Paleogene (Greenwood and Wing, 1995; Wilf, 2000; Greenwood et al., 2005; Eberle et al., 2010). However, most of these studies are restricted to a few, well-sampled regions (e.g. western North America) and provide only a ‘snapshot’ of climate (Fricke and Wing, 2004; Greenwood et al., 2005). As a result, the spatial and temporal evolution of terrestrial temperature change during the early Eocene remains poorly constrained. For example, there is currently no terrestrial temperature estimate for the early Eocene in Europe.

The MBT/CBT proxy (methylation of branched tetraethers/cyclisation of branched tetraethers; Weijers et al., 2007; Peterse et al., 2012) can also provide long-term, quantitative temperature records and is increasingly used to reconstruct terrestrial temperature during the early Paleogene (Pross et al., 2012; Pancost et al., 2013). The proxy is based upon the distribution of bacterial, soil-derived branched glycerol dialkyl glycerol tetraethers (brGDGTs), where the degree of methylation, expressed as the MBT’ ratio (methylation of branched tetraethers), is related to MAT and pH, and the number of cyclopentane rings, expressed as the CBT ratio (cyclisation of branched tetraethers), is related to soil pH (Weijers et al., 2007; Peterse et al., 2012). A new set of brGDGT isomers (6-methyl brGDGTs) have recently been identified and have enabled the development of more accurate pH and MAT calibrations (De Jonge et al., 2014a, 2014b). Although these new indices have not been applied in deep time investigations, previous iterations have been used to reconstruct terrestrial climate during the Quaternary (e.g. Sinnighe Damsté et al., 2012) and Paleogene (e.g. Pancost et al., 2013).

BrGDGTs are abundant in soils and peats; however, they are also transported via rivers and deposited in shallow continental shelves (Zell et al., 2014). As such, marginal marine sediments have been used to generate long-term continental temperature records during the geological record, especially during the early Palaeogene (e.g. Pross et al., 2012; Bijl et al., 2013; Pancost et al., 2013). However, recent work has highlighted challenges in its interpretation arising from uncertainty in the brGDGTs origin, with possible sources including *in-situ* production in the marine realm (Weijers et al., 2014), in rivers (Zell et al., 2014), in lakes (Weber et al., 2015) and in soils from the surrounding catchment (Bendle et al., 2010). Peats and lignites, in contrast, largely record *in-situ* environmental conditions and could provide unique new insights into terrestrial climate change.

However, the application of the brGDGT palaeothermometer in peat – and by extension lignite – can be complicated by additional effects on the brGDGT distribution (Weijers et al., 2011; Zheng et al., 2015). In modern settings, factors other than temperature and pH appear to influence brGDGT distributions (Weijers et al., 2011) and pH estimates are substantially higher than expected (Weijers et al., 2011), although these studies pre-date the recent advances in analytical techniques that allow for the separation of 5- and 6-methyl brGDGTs and do not utilise the most recent latest calibrations (De Jonge et al., 2014a, 2014b). Weijers et al. (2011) reported brGDGTs in one lignite sample from the late Palaeocene, but a more detailed and systematic study of branched GDGTs in lignites is lacking.

Here we examine brGDGT distributions in a series of thermally immature lignite seams from Germany inferred to represent ancient ombrotrophic bog deposits (Riegel et al., 2012; Inglis et al., 2015a). Sediments were recovered from Schöningen, central Germany (~48°N palaeolatitude) and were deposited through the early Eocene (Riegel et al., 2012; Robson et al., 2015). We investigate the distribution of brGDGTs within these ancient peat-forming environments and assess the impact of vegetation upon brGDGT distributions. We then provide the first terrestrial temperature record from central-western continental Europe through

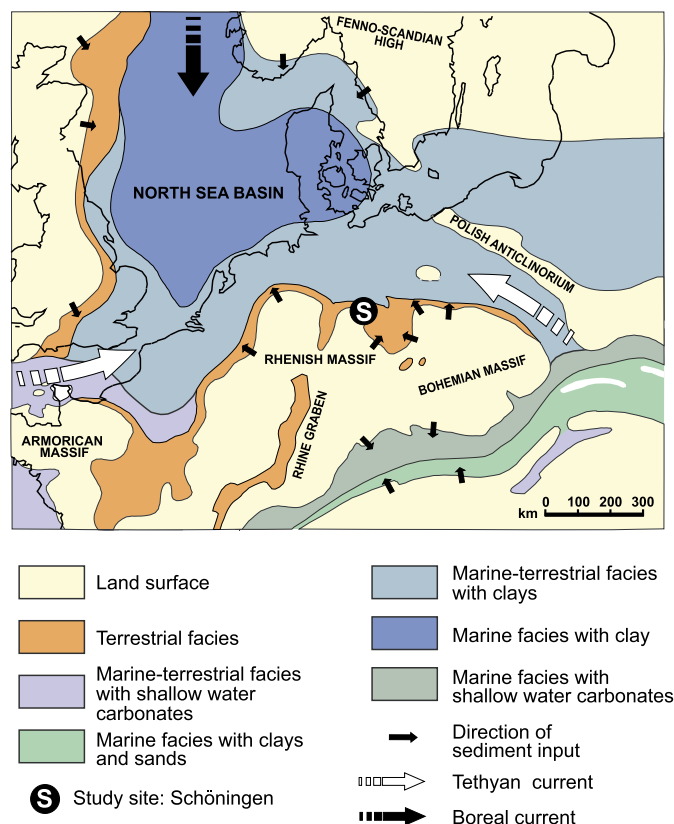


**Fig. 1.** Paleogeography of NW Europe during the early Eocene showing the location of Schöningen (modified from Riegel et al., 2012). (For interpretation of the references to color in this figure legend, the reader is referred to the web version of this article.)

the early Eocene and compare this with other terrestrial climate records as well as a range of climate model simulations. In order to investigate the most likely driving mechanism of early Paleogene climate change, we also compare our results with climate model simulations spanning multiple CO<sub>2</sub> concentrations.

## 2. Methods

### 2.1. Site description

#### 2.1.1. Schöningen Südfeld mine

Samples were collected from the Schöningen Südfeld mine (52.1333°N, 10.9500°E) in northern Germany, NW Europe (Fig. 1). Sediments were deposited in a low lying coastal setting at the southern shore of the North Sea (~48°N palaeolatitude) (Riegel et al., 2012). The Schöningen Formation comprises 10 lignite seams, from the Main Seam to the base of Seam 9, with intercalated nearshore shallow marine deposits. Dinocyst zone D5b (~55–56 Ma) was previously recognised above Main Seam in the nearby Emmerstedt area (Ahrendt et al., 1995). If Main Seam is coeval at both Schöningen and Emmerstedt, this would indicate that Seam 1 at Schöningen is earliest Eocene and that the Paleocene–Eocene boundary would be within Main Seam or below. However, within Interbed 2, above Seam 1, there is a dramatic increase in the abundance of the dinocyst *Apectodinium* (Riegel et al., 2012) which may represent the onset of the Paleocene–Eocene Thermal Maximum (PETM) as it does at other sites. As such, this would indicate that both Main Seam and Seam 1 are latest Paleocene. Based upon these observations, Main Seam and Seam 1 could be either latest Paleocene or earliest Eocene.

Two lines of evidence tentatively place Seam 4 and/or Seam 5 within or near to the EECO. Firstly, within Seam 4 there is a

sudden increase of palm pollen (*Monocolpollenites tranquilus*), the only significant palynological innovation within the section (Riegel et al., 2012). Secondly, within Seam 5 there is a significant increase in inertinite percentages (i.e. an increase in wildlife; Robson et al., 2015).

Ahrendt et al. (1995) identified dinoflagellate zone D9a in boreholes from the Emmerstedt area at levels both below and above a horizon they correlated with the Emmerstedter Grünsand at the top of the lower seam group at Schöningen. Zone D9a is calibrated to Chron C22r and is within the late Ypresian (49.9–52.8 Ma; GTS2012). Assuming that the lower seam group in the Emmerstedt and Helmstedt area (some 12 km north east of Schöningen) is coeval with the lower seam group at Schöningen (with the Emmerstedter Grünsand either being missing or replaced by interbed 9 at Schöningen; Riegel et al., 2012) then the uppermost seam (Seam 9) studied in this paper is likely to be within the late Ypresian. Although there are uncertainties, we treat Seam 9 as late Ypresian in this paper (see also Robson et al., 2015).

High-resolution sampling ( $n = 40$ ) was performed on a ~2.7 m thick lignite seam (Seam 1). Assuming average peat-to-lignite compaction ratios of 4:1 and average tropical and subtropical peat accumulation rates of 2 mm/yr and 0.8 mm/yr, respectively (Collinson et al., 2009), Seam 1 likely spans between 5.4 and 13.5 kyr. Lower-resolution sampling ( $n = 22$ ; up to 5 per seam; Supplementary Information) was also carried out on nine lignite seams within the Schöningen mine (Main Seam, Seam 3, 4, 5, 6, L, 7, 8 and 9). Details of the seams, including field images and lithological logs are provided in the supplementary file to Robson et al. (2015). Samples were also taken from the underlying and overlying nearshore shallow marine interbed sediments ( $n = 18$ ; up to 4 per interbed; Supplementary Information).

## 2.2. Organic geochemistry

For the Schöningen lignite deposits and related sediments, approximately 0.5–10 g of sediment were extracted via Soxhlet apparatus for 24 h using dichloromethane (DCM):methanol (MeOH) (2:1 v/v) as the organic solvent. The total lipid extract (TLE) was initially separated over silica into neutral and fatty acid fractions using chloroform-saturated ammonia and chloroform:acetic acid (100:1 v/v), respectively (see Inglis et al., 2015a). The neutral fraction was subsequently fractionated over alumina into apolar and polar fractions using hexane:DCM (9:1 v/v) and DCM:MeOH (1:2 v/v), respectively.

The polar fraction, containing the GDGTs, was dissolved in hexane/*iso*-propanol (99:1, v/v) and passed through 0.45  $\mu\text{m}$  PTFE filters. Fractions were analysed by high performance liquid chromatography/atmospheric pressure chemical ionisation – mass spectrometry (HPLC/APCI-MS). Samples were analysed to separate 5-methyl and 6-methyl brGDGTs (Hopmans et al., 2016). Normal phase separation was achieved using two Waters Acquity UPLC BEH HILIC (2.1  $\times$  150 mm; 1.7  $\mu\text{m}$  i.d.) with a flow rate of 0.2 ml min<sup>-1</sup>. Samples were eluted isocratically with 78% A and 18% B for 25 min followed by a linear gradient to 35% B over 25 min, then a linear gradient to 100% B in 30 min, where A = hexane and B = hexane:IPA (9:1, v/v) (Hopmans et al., 2016). This method yields improved resolution of all critical GDGT pairs compared to previously reported chromatographic methods (Weijers et al., 2007). Analyses were performed in selective ion monitoring mode (SIM) to increase sensitivity and reproducibility and M + H<sup>+</sup> (protonated molecular ion) GDGT peaks were integrated.

### 2.2.1. Branched GDGT indices

The CBT and MBT' indices from Peterse et al. (2012) are:

$$\text{CBT} = -\log\left(\frac{(\text{Ib} + \text{IIb} + \text{IIb}')}{(\text{Ia} + \text{IIa} + \text{IIa}')}\right) \quad (1)$$

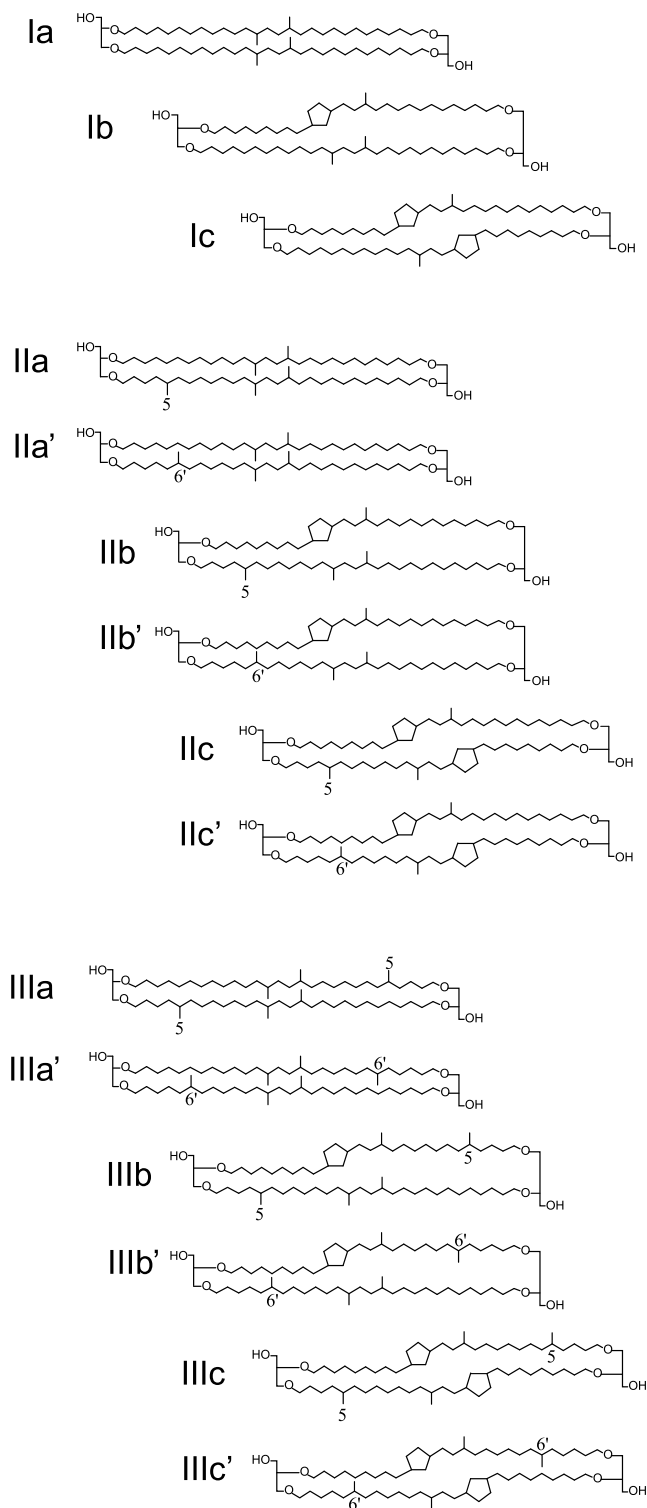


Fig. 2. Branched glycerol dialkyl glycerol tetraethers used to calculate MBT', CBT and related indices. 6-methyl branched GDGTs denoted by a dash.

$$\text{MBT}' = \frac{(\text{Ia} + \text{Ib} + \text{Ic})}{(\text{Ia} + \text{Ib} + \text{Ic} + \text{IIa} + \text{IIa}' + \text{IIb} + \text{IIb}' + \text{IIc} + \text{IIc}' + \text{IIIa} + \text{IIIa}')} \quad (2)$$

Roman numerals refer to individual GDGT structures shown in Fig. 2. In brief, I, II and III represent the tetra-, penta- and hexa-methylated components, respectively, and a, b and c represent the brGDGTs bearing 0, 1 or 2 cyclopentane moieties. 6-methyl brGDGTs are indicated by an apostrophe (e.g. IIa'). Equations (1)



and (2) have been expanded to show the 5-methyl (i.e. IIa) and 6-methyl (i.e. IIa') brGDGTs that were analysed as co-eluting compounds in the original MBT(')-CBT papers (Weijers et al., 2007; Peterse et al., 2012). Peterse et al. (2012) correlate CBT to pH using the calibration equation:

$$\text{pH} = 7.9 - 1.97 \cdot \text{CBT} \quad (r^2 = 0.70, n = 176, \text{RMSE} = 0.8). \quad (3)$$

The MBT'-CBT index is subsequently translated into temperature using the calibration equation (Peterse et al., 2012):

$$\text{MAT} (^{\circ}\text{C}) = 0.81 - 5.67 \cdot \text{CBT} + 31 \cdot \text{MBT}' \quad (r^2 = 0.59, n = 176, \text{RMSE} = 5.0 ^{\circ}\text{C}) \quad (4)$$

Recently, the separation of 5-methyl and 6-methyl brGDGTs has enabled the development of other pH and MAT equations (De Jonge et al., 2014a, 2014b). The CBT' index, which includes a combination of 5- and 6-methyl brGDGTs, is calculated using an objective statistical approach and yielded the strongest correlation with pH and is defined as (De Jonge et al., 2014a, 2014b):

$$\text{CBT}' = \log\left(\frac{\text{Ic} + \text{IIa}' + \text{IIb}' + \text{IIc}' + \text{IIIa}' + \text{IIIb}' + \text{IIIc}'}{\text{Ia} + \text{IIa} + \text{IIIa}}\right) \quad (5)$$

$$\text{pH} = 7.15 + 1.59 \cdot \text{CBT}' \quad (r^2 = 0.85, n = 221, \text{RMSE} = 0.52). \quad (6)$$

The highest correlation with MAAT and lowest residual error was achieved using multiple linear regression analysis and yields the following equation (De Jonge et al., 2014a, 2014b):

$$\text{MAT}_{\text{mr}} = 7.17 + 17.1 \cdot \text{Ia} + 25.9 \cdot \text{Ib} + 34.4 \cdot \text{Ic} - 28.6 \cdot \text{IIa} \quad (r^2 = 0.68, n = 222, \text{RMSE} = 4.6 ^{\circ}\text{C}). \quad (7)$$

The Branched vs. Isoprenoidal Tetraether (BIT) index, which is thought to represent the relative input of terrestrial-derived organic matter into the marine realm (Hopmans et al., 2004), is defined as:

$$\text{BIT} = \frac{\text{Ia} + \text{IIa} + \text{IIa}' + \text{IIIa} + \text{IIIa}'}{\text{Ia} + \text{IIa} + \text{IIa}' + \text{IIIa} + \text{IIIa}' + \text{Crenarchaeol}} \quad (8)$$

Equation (8) includes the 5-methyl (i.e. IIa) and 6-methyl (i.e. IIa') brGDGTs that were analysed as co-eluting compounds in the original BIT papers (Hopmans et al., 2004).

### 2.3. Modelling set-up

We compare terrestrial temperature estimates for Schöningen with published simulations of the early Eocene carried out using fully dynamic atmosphere-ocean GCMs of different complexities. These simulations include the EoMIP ensemble (Lunt et al., 2012) as well as more recent simulations (Kiehl and Shields, 2013; Sagoo et al., 2013). We also generate new simulations using HadCM3L fully coupled Atmosphere-Ocean General Circulation model (AOGCM), which is a version of the UKMO Unified Model HadCM3 (Gordon et al., 2000) but with lower resolution in the ocean. The atmospheric and oceanic components of the model comprise a resolution of 2.5° by 3.75°, with 19 vertical levels in the atmosphere and 20 vertical levels in the ocean. A single timeslice simulation (entitled HadCM3L-2; Table S5) was constructed for the Ypresian (56.0–47.8 Ma) utilising high resolution paleogeographic boundary conditions (Lunt et al., 2016) and run for 1422 model years in total to allow surface conditions to approach equilibrium, reducing the error arising from incomplete model spin-up relative to shorter simulations. Mean climate state is produced from the final 30 years of the simulation. Atmospheric CO<sub>2</sub> is prescribed a) 560 ppmv (2× Pre-Industrial level (PI)) and

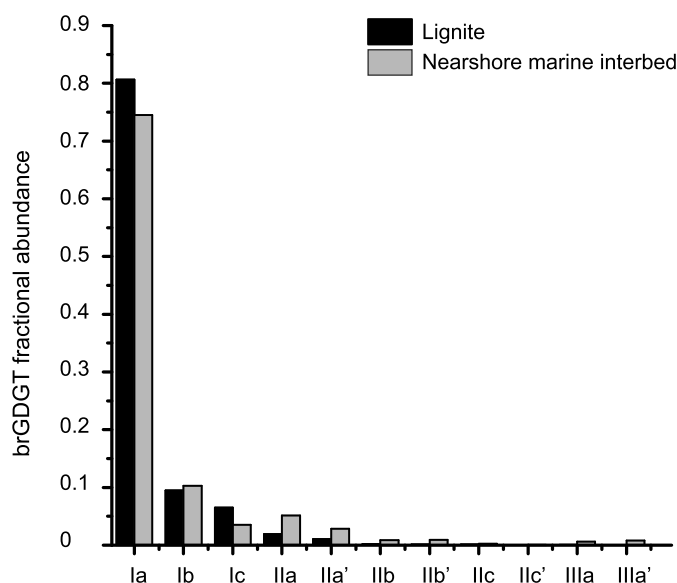


**Fig. 3.** The average fractional abundance of 5- and 6-methyl branched GDGTs within a typical lignite deposit (black) and the nearshore shallow marine interbeds (grey), using Seam 1 as an example. Roman numerals refer to structures shown in Fig. 2. 6-methyl branched GDGTs denoted by a dash.

b) 1120 ppmv (4× PI). For each simulation an appropriate solar constant representative of the Ypresian is defined. The barotropic solver in the ocean model requires the definition of continental islands, around which the net ocean flow is non-zero (see Inglis et al., 2015b). Note that Antarctica has not been defined as an island in any of these simulations, resulting in a net ocean flow of zero around Antarctica, even though the palaeogeographic reconstruction implies a possible pathway for circum-Antarctic transport. Indeed, the resolution of model is too coarse and the gateway too small to allow the definition of an island in the Ypresian. More details of the model setup are described in Lunt et al. (2016). In addition, we also include a revised version of HadCM3L, in which some of the parameters in the parameterisation scheme in the model have been modified following Sagoo et al. (2013) who perturbed parameters in the FAMOUS model and Irvine et al. (2013) who perturbed parameters in HadCM3. The most important parameters of this simulation (HadCM3L-3; Table S5) modified were related to cloud cover and resulted in reduced high latitude cloud and associated warming of polar regions.

## 3. Results

### 3.1. Branched GDGT distributions in Schöningen sediments

Within both the lignite and nearshore marine interbeds, the brGDGT distribution is dominated by tetramethylated brGDGTs which comprise ~95% of the total brGDGT assemblage (Fig. 3). The most abundant is brGDGT-Ia which makes up ~80% of the total brGDGT assemblage (Fig. 3). 6-methyl brGDGTs, which co-elute with 5-methyl brGDGTs in previous methods (e.g. Peterse et al., 2012), comprise only ~2–3% of the total brGDGT assemblage (Fig. 3). Of the 6-methyl brGDGTs, the pentamethylated brGDGT-IIa' is the most abundant. brGDGTs-IIb', -IIc', -IIIa', -IIIb' and -IIIc' are typically absent. The low fractional abundance of 6-methyl isomers can be attributed to 1) the dominance of tetramethylated brGDGTs which do not have a methyl group at the C-5 or C-6 position and 2) the relatively acidic and water saturated depositional environment which is associated with a low fractional abundance of 6-methyl brGDGTs in the global soil dataset (De Jonge et al., 2014a; Dang et al., 2016, respectively). A similar brGDGT distribution is

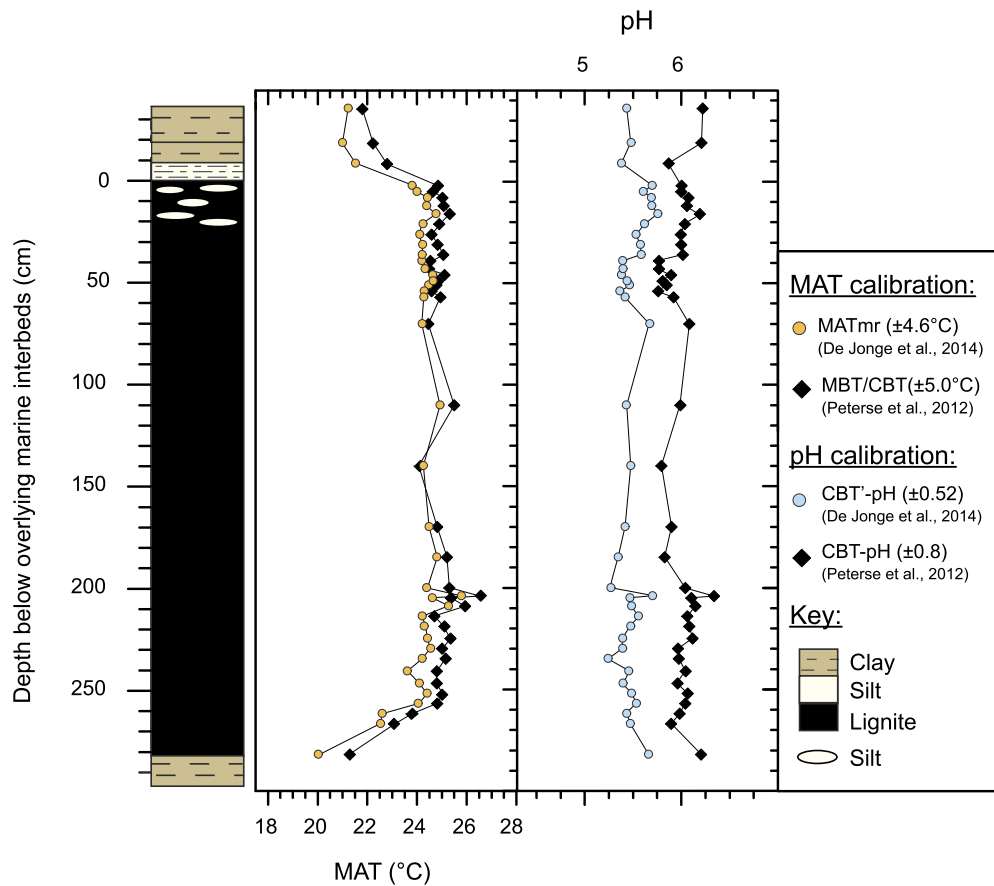


**Fig. 4.** Branched GDGT-derived mean air temperature (MAT) and pH estimates within Seam 1 and the overlying and underlying nearshore shallow marine interbeds. Calibrations derived from Peterse et al. (2012) (diamonds; Eq. (3)–(4)) and De Jonge et al., 2014a, 2014b (circles; Eq. (6)–(7)). (For interpretation of the references to color in this figure legend, the reader is referred to the web version of this article.)

noted for both the lignite and intercalated marine interbeds (see Fig. 3).

### 3.2. Branched GDGT ratios and MAT and pH trends

We restrict the following discussion to the indices and calibrations which exhibit the highest correlation with modern MAT ( $MAT_{mr}$ ; Eq. (7)) and soil pH (CBT; Eq. (5)–(6)). Results from previous indices and calibrations outlined in Peterse et al. (2012; see Eq. (1)–(4) above) are presented in the supplementary information (Tables S2–3).

High-resolution sampling within Seam 1 (latest Paleocene/earliest Eocene in age) indicates that  $MAT_{mr}$  estimates are relatively stable with depth in a single seam and range from  $\sim 23$  to  $26^\circ\text{C}$  (Fig. 4).  $MAT_{mr}$  estimates between Main Seam and Seam 9 span a similar range ( $\sim 23$  and  $25^\circ\text{C}$ ) during the early Eocene and exhibit  $<2^\circ\text{C}$  warming between Main Seam and Seam 1 (Fig. 5).  $MAT_{mr}$  estimates derived from marine nearshore interbed sediments, underlying and overlying the lignite seams, are consistently lower ( $\sim 19$  to  $24^\circ\text{C}$ ) and exhibit  $\sim 2$ – $3^\circ\text{C}$  of warming between Main Seam and Seam 3 (Fig. 5).

High-resolution sampling within Seam 1 indicates that pH estimates are relatively stable and range from 5.3 to 5.8 (Fig. 4). Between Main Seam and Seam 9, lignite-derived pH estimates range from 4.9 to 5.5 and exhibit no long-term trends (Fig. 5). pH estimates derived from the underlying and overlying marine interbed sediments are similar and range from  $\sim 4.8$  to 5.5. Similar to the lignite beds, they exhibit no long-term trends.

### 3.3. BIT indices

High-resolution sampling within Seam 1 indicates a minor decrease in BIT indices towards the top of Seam 1 (from 0.99 to 0.95) and is driven by a decrease in brGDGT concentrations rather than an increase in crenarchaeol. Between Main Seam and Seam 9, lignite-derived BIT indices range from 0.98 to 1.00. Within the underlying and overlying marine interbeds, the BIT index is lower, ranging from 0.94 to 0.98. In all samples, BIT indices are  $>0.9$ , indicating that the majority of GDGTs, and by extension organic matter, is terrestrial-derived.

## 4. Discussion

Within the Schöningen Formation ( $48^\circ\text{N}$ ), our MAT estimates average  $24^\circ\text{C}$  during the early Eocene ( $\sim 56$ – $50$  Ma). These values are consistent with palaeobotanical MAT estimates from similar palaeolatitudes ( $\sim 45^\circ\text{N}$ ) in western North America which range between  $20$  and  $25^\circ\text{C}$  during the late Paleocene and early Eocene (Huber and Caballero, 2011 and references therein), and from the late Ypresian at Messel, Germany ( $22$ – $24^\circ\text{C}$ ) (Grein et al., 2011; Lenz et al., 2014). The temperatures are also consistent with the high proportion of faunal fossils in the early Paleogene of western and central Europe whose nearest living relatives are thermophilic (Collinson and Hooker, 2003) including those of Messel. Our initial results therefore indicate the feasibility of brGDGT palaeothermometry in lignites. However, observations from modern peat-forming environments (e.g. Weijers et al., 2011; Zheng et al., 2015) indicate that there are a number of caveats which merit further exploration.

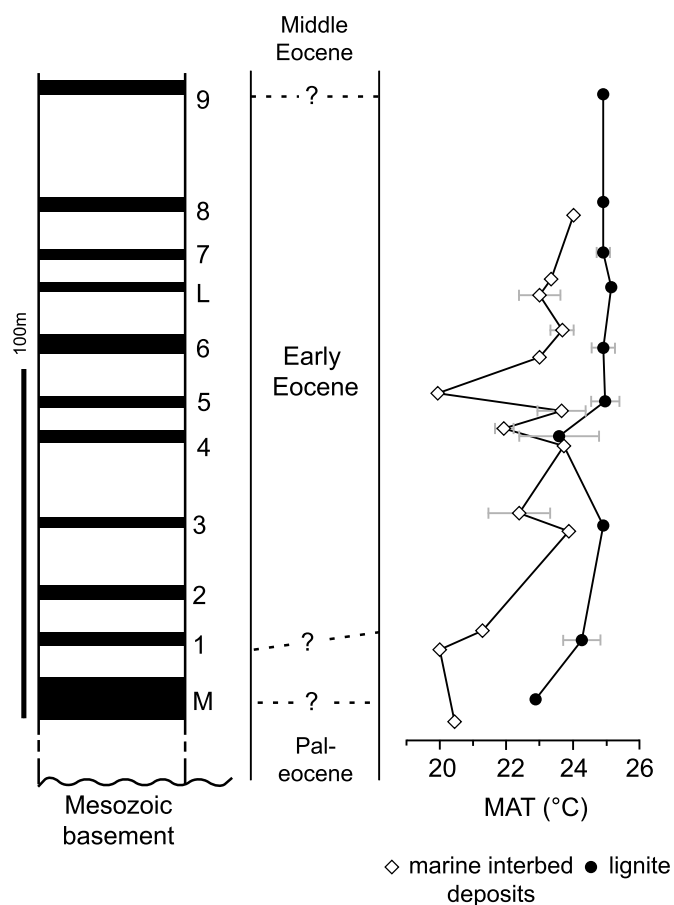


**Fig. 5.** MAT estimates through the Early Eocene at Schöningen. The age model follows Robson et al. (2015). MAT estimates shown from the nearshore marine interbeds (open diamond) are obtained below and/or above the corresponding lignite seams (closed circle). Where multiple samples were analysed, the standard deviation is shown (grey). No samples were obtained from Seam 2. For lignite and interbed sample numbers, refer to Supplementary Tables 1–3. For details of seams, interbeds, lithological logs, field photographs and lithologies refer to the supplementary material in Robson et al. (2015).

#### 4.1. Testing the fidelity of brGDGT palaeothermometry in lignite deposits

##### 4.1.1. Modern, recent or ancient deposition?

Previous studies have shown that bacteria can live in subsurface environments, including in lignites and coal beds (Inagaki et al., 2015). However, we consider this unlikely to have influenced our data at Schöningen for a number of reasons. Firstly, the total number of prokaryotic cells in subsurface lignite seams is typically several orders of magnitude lower than in most terrestrial settings (Inagaki et al., 2015). Secondly, the distribution of brGDGTs within Schöningen – an acidic, tropical peatland (Riegel et al., 2012; Inglis et al., 2015a) – is very similar to what has been observed in modern acidic, tropical peatlands (Naafs et al., in revision). Thirdly, if brGDGTs were derived from modern or recent deposition, we would expect much lower reconstructed temperatures (e.g. modern MATs at Schöningen are 8 °C). However, MATs always exceed 20 °C and are consistent with other early Eocene mid-to-high latitude palaeotemperature estimates (see Pancost et al., 2013; Wilf, 2000; Fricke and Wing, 2004; Bijl et al., 2013; and previous paragraph herein). Finally, in a previous study, there were no intact polar lipid GDGTs detected within a ca. 2 km thick interbedded lignite deposit, therefore arguing against an active GDGT-producing microbial community in these settings (Fry et al., 2009). In the same study, downcore profiles of core GDGT and intact phospho-

lipid concentrations diverge, suggesting the absence of significant subsurface GDGT production (Fry et al., 2009). Although we cannot fully exclude a subsurface contribution, we argue that modern and recent subsurface production is unlikely to have had an impact on the ancient brGDGT distributions in this setting.

##### 4.1.2. Influence of thermal maturity upon brGDGT palaeothermometry

Total hopane  $\beta\beta/(\beta\beta + \alpha\beta + \beta\alpha)$  ratios are relatively high (0.46–0.81; Inglis et al., 2015a), indicating that the samples are relatively immature and that MBT/CBT values are not biased by changes in thermal maturity (Schouten et al., 2013). Low maturation is also supported by the presence of uncompact palm stumps and *in-situ* preserved seagrass-like macrofossils (Riegel et al., 2012) which preclude a very thick overburden. Likewise, huminite reflectance and fluorescence spectra of sporinite from 11 samples at the nearby Helmstedt mine (Helmstedt Formation, about equivalent to seam 9 at Schöningen) range between 0.24 and 0.35, while maxima of fluorescence spectra vary between 510 and 536 nm. Both values are well within the lower part of the lignite rank and indicate very immature conditions.

##### 4.1.3. Influence of changes in vegetation on brGDGT palaeothermometry

Previous work suggested that major changes in vegetation can influence the distribution of brGDGTs in peat-forming environments, and therefore the reconstructed environmental parameters. For example, a change in CBT values, from  $\sim 0.3$  to  $\sim 1.6$ , coincides with an early Holocene transition from a *Carex*-dominated fen to a *Sphagnum*-dominated bog in Switzerland (Weijers et al., 2011). This corresponds to an estimated pH change of  $\sim 4$  units and a large drop in MBT/CBT-derived MAT estimates ( $\sim 15$  °C; Weijers et al., 2011). Within Seam 1, Schöningen, we apply biomarker and palynological proxies (Inglis et al., 2015a), to investigate the impact of vegetation change upon brGDGT-derived MAT estimates.

Within Seam 1, Schöningen, the dominant plant types represented by palynomorphs are ferns (e.g. *Laevigatosporites*), swamp-dwelling conifers (e.g. *Inaperturopollenites*), mixed mesophytic forest vegetation (e.g. *Tricolporopollenites cingulum*) and *Sphagnum* moss, as indicated by the abundance of *Sphagnum*-type spores (especially *Tripunctisporis*, originally used as a subgenus of the widely used but invalid genus *Stereisporites*; see Riegel and Wilde, 2016). Although the latter is typically associated with modern boreal and subarctic settings, abundant *Sphagnum* spores have also been found in other mid-latitude early Paleogene settings (see Riegel and Wilde, 2016). Sedges, which are well-represented in Europe from the Paleocene onwards, are not recorded in the dispersed palynological assemblages from Schöningen. This may be a genuine absence or may be due to a taphonomic bias against sedge pollen preservation. Thus, although sedges are a common plant in modern peat-forming environments we are not able to evaluate their role in the Schöningen vegetation.

The relative abundance of *Sphagnum*-type spores varies markedly within Seam 1 (Fig. 6d). *Sphagnum*-type spores are low or absent within the base of Seam 1 (200–267 cm; <10%; Fig. 6). This is consistent with previously published low  $C_{23}/C_{31}$  *n*-alkane values ( $\sim 0.4$ ) (Inglis et al., 2015a) and indicates that *Sphagnum* moss was probably not an important component of the peat-forming vegetation within this interval (Fig. 6). An increase in waterlogged conditions towards the top of Seam 1 (57–0 cm) coincides with the proliferation of *Sphagnum*-type spores (Fig. 6). The  $C_{23}/C_{31}$  *n*-alkane ratio also increases and yields values that are typical of a modern, *Sphagnum*-dominated bog (Fig. 6c) (Inglis et al., 2015a). Although *Sphagnum* expansion is associated with a decrease in the fractional abundance of brGDGT-Ia, from 0.84 to 0.76, MAT and pH estimates remain stable throughout Seam 1 (Fig. 6). This trend is observed regardless of the calibration (Weijers et al., 2007; Peterse et al., 2012; De Jonge et al., 2014a, 2014b) and indi-

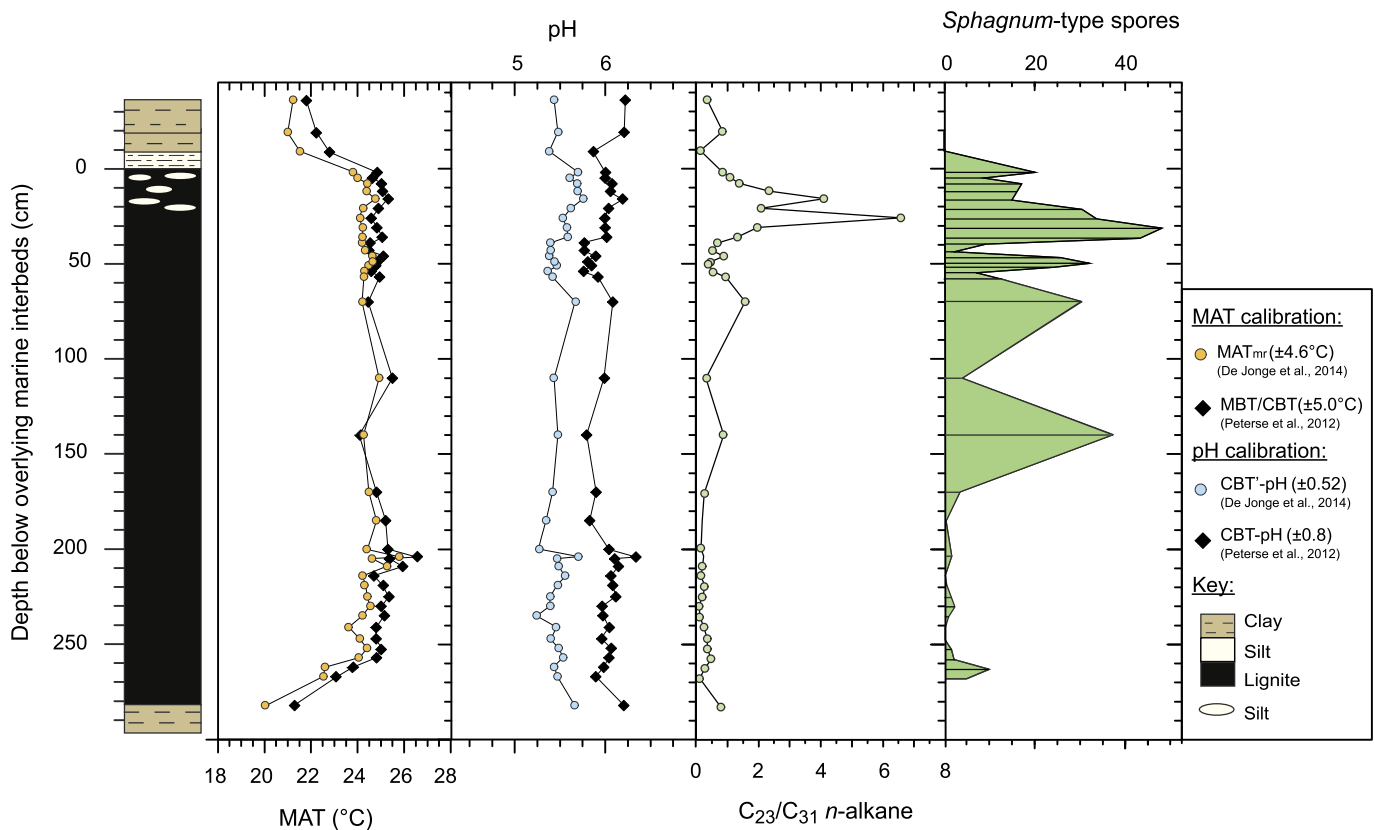


**Fig. 6.** No effect of vegetation change to brGDGT indices within Seam 1. a) Mean air temperature (MAT) estimates, b) pH estimates, c) the  $C_{23}/C_{31}$  *n*-alkane ratio (a proxy for *Sphagnum* input) and d) the relative abundance (total palynomorphs) of *Sphagnum*-type spores. (For interpretation of the references to color in this figure legend, the reader is referred to the web version of this article.)

cates that brGDGT-derived MAT (or pH) estimates from Seam 1 at Schöningen are not biased by changes in vegetation.

Revisiting Weijers et al. (2011), it is clear that MAT estimates across the transition from a *Carex*-dominated fen to *Sphagnum*-dominated bog were skewed by the overly strong impact of the pH correction upon the MBT-CBT proxy. As the most recent MAT calibration no longer requires a pH correction (De Jonge et al., 2014a, 2014b), MAT estimates are unlikely to be as severely impacted by vegetation change in future studies. Indeed, within an ombrotrophic bog from Switzerland, the transition from *Sphagnum*-dominated bog to mixed *Sphagnum*/*Eriophorum* vegetation is not associated with a change in brGDGT-derived MAT or pH estimates (Weijers et al., 2011). This indicates that vegetation change is less of a concern than originally inferred in Weijers et al. (2011).

#### 4.1.4. Influence of lithological change upon brGDGT palaeothermometry

Within the Schöningen Formation,  $MAT_{mr}$  estimates from within the lignite seams are consistently warmer ( $\sim 2$ – $4$  °C) than those from the associated nearshore shallow marine interbed sediments (Fig. 5). The differences exist regardless of the calibration (Weijers et al., 2007; Peterse et al., 2012; De Jonge et al., 2014a), because they arise from differences in the distribution of the major brGDGTs common to all calibrations. Specifically, the nearshore shallow marine sedimentary deposits are characterised by a lower fractional abundance of tetramethylated brGDGTs and a higher fractional abundance of pentamethylated and hexamethylated brGDGTs.

A systematic offset in MAT estimates between the lignite and nearshore shallow marine interbed sediments could record a genuine temperature signal, where warming promotes sea level rise and the deposition of shallow marine deposits. However, this

should be associated with an increase (rather than decrease) in shallow marine MAT estimates. Previous studies have shown that there is an increase in MBT/CBT-derived MAT estimates within the oxidised section of a turbidite deposit (Lengger et al., 2013). This is related to the preferential degradation of *in-situ*, marine-derived, brGDGTs compared to the more recalcitrant terrestrial-derived brGDGTs (Lengger et al., 2013). However, we do not expect this to be an important factor in our setting as the majority of organic matter is terrestrial-derived, as indicated by high BIT indices ( $>0.9$ ) and the presence of higher plant biomarkers.

Instead, the temperature difference could reflect different sources of the respective brGDGTs. A decrease in  $MAT_{mr}$  estimates within the nearshore marine interbeds could reflect a higher altitude source region (Bendle et al., 2010). However, this is unlikely as Schöningen was low-lying and subsequently flooded during the early Oligocene transgression (Standke, 2008). An alternative difference in source could arise from partial *in-situ* production of brGDGTs in the marine sediments (Weijers et al., 2014). This typically only dominates the recorded temperature signature in settings characterised by low BIT values and Schöningen samples are characterised by high BIT indices ( $>0.9$ ) and an abundance of terrestrial palynomorphs and biomarkers (see Inglis et al., 2015a); as such, we suggest that *in-situ* marine production is unlikely to account for the observed temperature offset.

We suggest that this offset is related to changes in the source of the brGDGTs, with recent work suggesting *in-situ* production within river (De Jonge et al., 2014b; Zell et al., 2014) and lacustrine (Weber et al., 2015) systems. We suggest that these different settings (e.g. lacustrine, rivers) have different calibrations/controls that give rise to slight temperature differences in the sedimentary record. Indeed, the occurrence of large scale cross-bedded sands overlying Seam 6 and the presence of fluvial channels, freshwa-



ter phytoplankton (mainly *Botryococcus*), and freshwater dinocysts within Interbed 9 suggests proximity to fluvio-lacustrine environments (Riegel et al., 2012).

#### 4.1.5. Investigating the upper limit of the brGDGT palaeothermometer

The global soil dataset used to develop the brGDGT palaeotemperature proxy spans a wide temperature range; however, it does not include samples  $>27^{\circ}\text{C}$ , potentially complicating the application of this proxy in low-latitude 'greenhouse' climates. Although the  $\text{MAT}_{\text{mr}}$  index has a theoretical maximum temperature of  $\sim 41^{\circ}\text{C}$  (De Jonge et al., 2014a, 2014b), this temperature can only be obtained when the brGDGT distribution is composed exclusively of brGDGT-Ic (see Table S4). As this distribution has not been observed in natural samples – and in fact, tropical peats are dominated by Ia rather than Ic – the upper limit of the  $\text{MAT}_{\text{mr}}$  index is likely much lower. For example, a hypothetical sample composed exclusively of brGDGT-Ia yields a  $\text{MAT}_{\text{mr}}$  estimate of  $24.3^{\circ}\text{C}$ . If earth system models that simulate early Eocene low-latitude MATs  $>35\text{--}40^{\circ}\text{C}$  are robust (e.g. CCSM3-W; see section 4.3 for a more detailed discussion), this implies that the application of the brGDGT palaeothermometer in low- and mid-latitude greenhouse requires careful consideration of calibration limits (see section 4.2).

#### 4.2. New insights into early Paleogene terrestrial temperature change

Within the Schöningen Formation, lignite-derived  $\text{MAT}_{\text{mr}}$  estimates range from  $23$  to  $26^{\circ}\text{C}$  (Fig. 5) and those derived from the nearshore marine interbed sediments typically exceed  $20^{\circ}\text{C}$  (Fig. 5). These results clearly indicate that central-western Europe was much warmer than modern (modern MAT:  $\sim 9^{\circ}\text{C}$ ). Enhanced warmth is consistent with other mid-latitude settings and a range of modelling simulations. These results also provide the first long-term terrestrial temperature record from western continental Europe through the early Eocene. In the basal part of the section studied (Main Seam to Seam 3), warming is recorded from both the lignites ( $\sim 2^{\circ}\text{C}$ ) and nearshore marine interbed sediments ( $2\text{--}3^{\circ}\text{C}$ ). During the subsequent early Eocene (Seam 3 upwards), there is a long-term temperature maximum recorded from both the lignites and nearshore marine interbeds. This may include the interval containing the Early Eocene Climatic Optimum (EECO) (Robson et al., 2015).

Although the magnitude of warming is within the calibration error ( $\pm 4.6^{\circ}\text{C}$ ), it is lower than the analytical error (Schouten et al., 2013). As such, this proxy has been used to reconstruct a similar magnitude of temperature change in other early Palaeogene settings (Bijl et al., 2013; Pancost et al., 2013) and in Holocene studies (Sinninghe Damsté et al., 2012). Changes in the palynological assemblage also support increasing temperatures during the early Eocene. Specifically, there is a decrease in inaperturate (mostly taxodiaceous) pollen and temperate elements within the upper part of the formation and in some seams an increase in thermophilic elements, such as palms (e.g. *Monocolpopollenites tranquillus*) and tropical trees (e.g. *Tetracolporopollenites*) (Riegel et al., 2012). As such, our record likely records a genuine temperature signal. Indeed, as we may have reached upper limit of the proxy in some samples, the magnitude of warming observed is likely a minimum estimate.

The warming in the basal part of the section at Schöningen is consistent with other studies. For example, qualitative palaeobotanical evidence from Russia and Northern Kazakhstan indicates warming between the late Paleocene and the middle of the early Eocene (Akhmetiev, 2010). Within the Bighorn Basin, Wyoming, leaf margin analysis also indicates a warming trend from the late Paleocene to the early Eocene and a temperature maximum during the middle of the early Eocene ( $\sim 22\text{--}24^{\circ}\text{C}$ ) (Wilf, 2000; Fricke and Wing, 2004). Although the Bighorn Basin leaf-physiognomy study

suggests more pronounced warming between the earliest Eocene and EECO ( $\sim 4\text{--}7^{\circ}\text{C}$ ; Wilf, 2000), the overall trends are consistent. Clumped isotope ( $\Delta_{47}$ ) temperature measurements from paleosol carbonates in the Bighorn Basin during the late Paleocene and early Eocene have been interpreted to reflect summer temperatures (Snell et al., 2013), but they also indicate net warming from the late Paleocene to the middle of the early Eocene.

In the SW Pacific, MBT/CBT-derived MAT temperature estimates obtained from marginal marine sediments indicate warming from the earliest Eocene ( $\sim 56/55$  Ma) to the EECO (Bijl et al., 2013; Pancost et al., 2013). These results also indicate a terrestrial temperature maximum ( $\sim 19\text{--}22^{\circ}\text{C}$ ) during the EECO throughout the SW Pacific, with evidence from Mid-Waipara River ( $\sim 55^{\circ}\text{S}$ ; Pancost et al., 2013), ODP Site 1172 ( $\sim 65^{\circ}\text{S}$ ; Bijl et al., 2013) and IODP Site 1356 ( $\sim 67^{\circ}\text{S}$ ; Pröss et al., 2012). Collectively, these results indicate that both the northern and southern hemisphere were characterised by long-term terrestrial warming during the late Paleocene and early Eocene with a temperature maximum during the middle of the early Eocene.

There is additional evidence from the marine realm that suggests similar patterns of warming. In the northern hemisphere,  $\text{TEX}_{86}$  SST estimates from the Western Siberian Sea (Frieling et al., 2014) indicate a  $\sim 4\text{--}6^{\circ}\text{C}$  increase in SSTs between the earliest Eocene ( $\sim 55\text{--}54$  Ma) and EECO, while in the SW Pacific  $\text{TEX}_{86}$  SST estimates indicate a  $\sim 4\text{--}6^{\circ}\text{C}$  increase between the earliest Eocene ( $\sim 55$  Ma) and EECO (Hollis et al., 2012; Bijl et al., 2013; Inglis et al., 2015b). In comparison to the terrestrial realm, the magnitude of ocean warming is typically greater. The reason for this is unclear but may suggest decoupling between the terrestrial and marine realm. A similar observation has been made for the middle and late Eocene in the SW Pacific (ODP 1172, HB and MW) and was attributed to regional oceanographic change (e.g. Pancost et al., 2013). However, it is also possible that the MBT/CBT-derived temperature signal is muted as values approach its upper limit.

#### 4.3. A regional data-model comparison at Schöningen

Reconciling proxy and model-derived temperature estimates during the early Eocene is challenging, with models often underestimating mid-to-high latitude warmth (see Lunt et al., 2012). However, recent work has shown congruence between certain models (i.e. CCSM3-H) and (terrestrial) data (Huber and Caballero, 2011). To explore this further, we compare our brGDGT-derived temperature estimates – which range between  $\sim 20^{\circ}\text{C}$  to  $26^{\circ}\text{C}$  – with a range of model simulations of differing complexities (HadCM3L, FAMOUS, GISS, ECHAM4.5 and CCSM3) run under different  $\text{CO}_2$  scenarios (560 to 4480 ppmv; Fig. 7; Table S5).

At the lower range of  $\text{CO}_2$  estimates ( $2\times$  PI; 560 ppm), two FAMOUS simulations (Fig. 7; E16 and E17 in Sagoo et al., 2013) reconstruct MAT estimates ( $\sim 24\text{--}25^{\circ}\text{C}$ ) for NW Germany that are similar to our proxy-derived estimates ( $\sim 20^{\circ}\text{C}$  to  $26^{\circ}\text{C}$ ). These simulations perturb a range of parameters including cloud and diffusion processes and simulate early Eocene warmth at lower  $p\text{CO}_2$  concentrations compared to HadCM3L, CCSM3 and ECHAM. For intermediate  $\text{CO}_2$  estimates, both CCSM3-K ( $5\times$  PI; 1400 ppm; Fig. 7) and HadCM3L-3 ( $6\times$  PI; 1680 ppm; Fig. 7) range between  $20$  and  $24^{\circ}\text{C}$  and are in agreement with proxy estimates at Schöningen ( $\sim 20^{\circ}\text{C}$  to  $26^{\circ}\text{C}$ ). The  $\text{CO}_2$  concentration prescribed in these experiments are consistent with early Eocene proxy  $p\text{CO}_2$  estimates ( $\sim 1400$  ppm; Anagnostou et al., 2016). At the higher range of  $\text{CO}_2$  estimates ( $16\times$  PI; 4480 ppm; Fig. 7), CCSM3-W and CCSM3-H temperature estimates closely match the data ( $21$  and  $26^{\circ}\text{C}$ , respectively). Although these  $\text{CO}_2$  estimates are much higher than indicated by proxy data, these values should only be interpreted as a tool in which to increase the radiative forcing in simulations with a weak sensitivity to warming (see Huber and Caballero, 2011). Col-

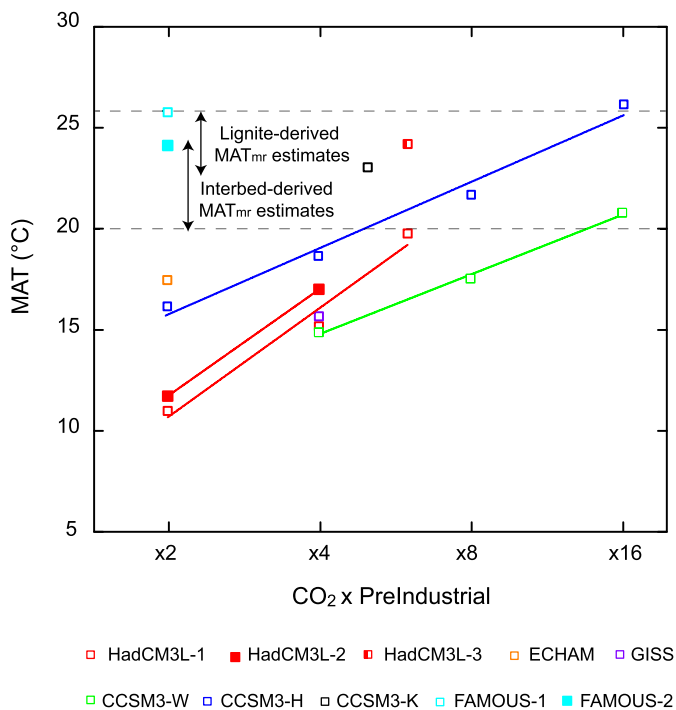


**Fig. 7.** Model-derived temperature estimates for Schöningen during the Early Eocene (~56–478 Ma). For full details on each model simulation, see Supplementary Table 5. (For interpretation of the references to color in this figure legend, the reader is referred to the web version of this article.)

lectively, these results indicate a strong agreement between several different models – albeit run under different  $p\text{CO}_2$  concentrations – and our brGDGT-derived MAT estimates, further supporting enhanced mid-latitude warmth during the early Eocene. Despite this, some models (e.g. GISS) still continue to underestimate our reconstructed temperatures (Fig. 7). In addition, we have focused on data-model comparison only for this site and different conclusions could be drawn from a global compilation.

Using some of these simulations, we can also explore whether a doubling of  $p\text{CO}_2$  can account for the magnitude of warming observed at Schöningen. For HadCM3L-1 and HadCM3L-2 simulations (see Table S5), atmospheric  $\text{CO}_2$  is prescribed at: a) 560 ppmv ( $2\times$  Pre-Industrial level (PI)) and b) 1120 ppmv ( $4\times$  PI). Although these values are consistent with early Paleogene proxy estimates, the simulations yield much colder absolute temperatures than would be anticipated for this site (e.g. HadCM3L-2:  $12^\circ\text{C}$  and  $17^\circ\text{C}$  for  $2\times$  PI and  $4\times$  PI, respectively; see Table S5). For CCSM3-W and CCSM3-H, atmospheric  $\text{CO}_2$  is prescribed at: a) 560 ppmv ( $2\times$  PI), b) 1120 ppmv ( $4\times$  PI), c) 2240 ppmv ( $8\times$  PI) and d) 4480 ppmv ( $16\times$  PI). The  $8\times$  and  $16\times$  PI simulations are higher than predicted for early Paleogene proxy  $\text{CO}_2$  estimates; however, these simulations yield temperatures which are most consistent with our brGDGT estimates (e.g. CCSM3-H:  $22^\circ\text{C}$  and  $26^\circ\text{C}$  for  $8\times$  PI and  $16\times$  PI, respectively; see Table S5).

On average, the HadCM3L simulations predict  $4.8^\circ\text{C}$  ( $\pm 0.8^\circ\text{C}$ ) of warming at Schöningen for a doubling of  $\text{CO}_2$  (Table S5) whereas CCSM3 predict  $\sim 3.3^\circ\text{C}$  ( $\pm 0.8^\circ\text{C}$ ) for the same scenario (Table S5). The CCSM3 simulations are consistent with the brGDGTs which indicate  $\sim 2$  to  $3^\circ\text{C}$  of warming between the latest Palaeocene/earliest Eocene (Main Seam to Seam 3) and middle Early Eocene (Seam 4 and 5). As this interval also coincides with an approximate twofold increase in  $\text{CO}_2$  estimates this may suggest that a doubling of  $p\text{CO}_2$  can account for the warming observed at Schöningen during the early Eocene. However, additional temperature records from other regions are required to evaluate this hypothesis.

## 5. Conclusions

Using samples recovered from Schöningen, central Germany ( $\sim 48^\circ\text{N}$  palaeolatitude), we provide the first detailed study into the occurrence and distribution of brGDGTs in a series of early Eocene lignite seams. brGDGTs are abundant within every sample and the distribution is dominated by tetramethylated brGDGTs. Unlike some Holocene peat studies, changes in vegetation do not affect MAT or pH estimates within Seam 1. However, variations in the depositional environment (lignites and interbed sediments) do yield small changes in MAT estimates. Using the most recent brGDGT temperature calibrations developed for soils, we present the first record of terrestrial temperature in central-western continental Europe through the early Eocene. MAT<sub>mr</sub> estimates range from 20 to  $26^\circ\text{C}$  and are consistent with other mid-latitude, early Eocene temperature records as well as some new and existing model simulations. In the basal part of the section studied, MATs in the lignite and marine interbed sediments increase by  $\sim 2\text{--}3^\circ\text{C}$  and culminate in a long-term temperature maximum, in a part of the sequence likely to include the Early Eocene Climatic Optimum (EEO). Although this trend is relatively well established in marginal marine sediments within the SW Pacific, it has rarely been shown in other regions. Using a range of climate models, our warming trend is consistent with a doubling of  $\text{CO}_2$  and broadly agrees with proxy-derived  $\text{CO}_2$  estimates from the early Paleogene. These results also indicate that brGDGT palaeothermometry could be applied to other lignites.

## Acknowledgements

The research leading to these results has received funding from the European Research Council under the European Union's Seventh Framework Programme (FP/2007–2013) / ERC Grant Agreement number 340923 (TGRES, awarded to RDP). We thank the NERC LSMSF (Bristol) for analytical support. GNI thanks the UK NERC for supporting his PhD studentship (NE/I005714/1). RDP acknowledges the Royal Society Wolfson Research Merit Award. MEC, BER and ACS gratefully acknowledge funding from NERC grant NE/J008656/1. ACS also acknowledges a Leverhulme Trust Emeritus Fellowship (EM-2012-054). DJL and AF acknowledge grants NERC grants Descent into the Icehouse (NE/I005714/1) and CPE (NE/K014757/1, NE/K012479/1) and thank Getech Plc for providing the Ypresian paleogeography. We thank Karin Schmidt (Senckenberg Forschungsinstitut und Naturmuseum, Frankfurt) for extensive logistical support, especially during field work and Ellen Hopmans (NIOZ) for helpful discussions. We are also thankful to 'Helmstedter Revier of MIBRAG' and previous owners of the mine for continued access to the Schöningen mine. Finally, we thank the two anonymous reviewers for their comments and thoughtful suggestions which greatly improved this manuscript.

## Appendix A. Supplementary material

Supplementary material related to this article can be found online at <http://dx.doi.org/10.1016/j.epsl.2016.12.009>.

## References

- Ahrendt, H., Köthe, A., Lietzow, A., Marheine, D., and Ritzkowski, S., 1995. Lithostratigraphie, Biostratigraphie und radiometrische Datierung des Untereozäns von Helmstedt (SE-Niedersachsen), Zeitschrift der deutschen geologischen Gesellschaft, pp. 450–457.
- Akhmetiev, M.A., 2010. Paleocene and Eocene floristic and climatic change in Russia and Northern Kazakhstan. Bull. Geosci. 85 (1), 17–34.
- Anagnostou, E., John, E.H., Edgar, K.M., Foster, G.L., Ridgwell, A., Inglis, G.N., Pancost, R.D., Lunt, D.J., Pearson, P.N., 2016. Changing atmospheric  $\text{CO}_2$  concentration was the primary driver of early Cenozoic climate. Nature 533 (7603), 380–384.

- Bendle, J.A., Weijers, J.W.H., Maslin, M.A., Sinninghe Damsté, J.S., Schouten, S., Hopmans, E.C., Boot, C.S., Pancost, R.D., 2010. Major changes in glacial and Holocene terrestrial temperatures and sources of organic carbon recorded in the Amazon fan by tetraether lipids. *Geochem. Geophys. Geosyst.* 11 (12), Q12007.
- Bijl, P.K., Bendle, J.A.P., Bohaty, S.M., Pross, J., Schouten, S., Tauxe, L., Stickley, C.E., McKay, R.M., Röhl, U., Olney, M., Sluijs, A., Escutia, C., Brinkhuis, H., Scientists, E., 2013. Eocene cooling linked to early flow across the Tasmanian Gateway. *Proc. Natl. Acad. Sci.* 110 (24), 9645–9650.
- Collinson, M.E., Hooker, J.J., 2003. Paleogene vegetation of Eurasia: framework for mammalian faunas. *Deinsea* 10, 41–83.
- Collinson, M.E., Steart, D.C., Harrington, G.J., Hooker, J.J., Scott, A.C., Allen, L.O., Glasspool, I.J., Gibbons, S.J., 2009. Palynological evidence of vegetation dynamics in response to palaeoenvironmental change across the onset of the Paleocene–Eocene Thermal Maximum at Cobham, Southern England. *Grana* 48 (1), 38–66.
- Dang, X., Yang, H., Naafs, B.D.A., Pancost, R.D., Xie, S., 2016. Evidence of moisture control on the methylation of branched glycerol dialkyl glycerol tetraethers in semi-arid and arid soils. *Geochim. Cosmochim. Acta*.
- De Jonge, C., Hopmans, E.C., Zell, C.I., Kim, J.-H., Schouten, S., Sinninghe Damsté, J.S., 2014a. Occurrence and abundance of 6-methyl branched glycerol dialkyl glycerol tetraethers in soils: implications for palaeoclimate reconstruction. *Geochim. Cosmochim. Acta* 141 (0), 97–112.
- De Jonge, C., Stadnitskaia, A., Hopmans, E.C., Cherkashov, G., Fedotov, A., Sinninghe Damsté, J.S., 2014b. *In situ* produced branched glycerol dialkyl glycerol tetraethers in suspended particulate matter from the Yenisei River, Eastern Siberia. *Geochim. Cosmochim. Acta* 125 (0), 476–491.
- Eberle, J.J., Fricke, H.C., Humphrey, J.D., Hackett, L., Newbrey, M.G., Hutchison, J.H., 2010. Seasonal variability in Arctic temperatures during early Eocene time. *Earth Planet. Sci. Lett.* 296 (3–4), 481–486.
- Fricke, H.C., Wing, S.L., 2004. Oxygen isotope and paleobotanical estimates of temperature and  $\delta^{18}\text{O}$ –latitude gradients over North America during the early Eocene. *Am. J. Sci.* 304 (7), 612–635.
- Frieling, J., Iakovleva, A.I., Reichart, G.-J., Aleksandrova, G.N., Gnidzenko, Z.N., Schouten, S., Sluijs, A., 2014. Paleocene–Eocene warming and biotic response in the epicontinental West Siberian Sea. *Geology* 42 (9), 767–770.
- Fry, J.C., Horsfield, B., Sykes, R., Cragg, B.A., Heywood, C., Kim, G.T., Mangelsdorf, K., Mildenhall, D.C., Rinna, J., Vieth, A., Zink, K.-G., Sass, H., Weightman, A.J., Parkes, R.J., 2009. Prokaryotic populations and activities in an interbedded coal deposit, including a previously deeply buried section (1.6–2.3 km) above ~150 Ma basement rock. *Geomicrobiol. J.* 26 (3), 163–178.
- Gordon, C., Cooper, C., Senior, C.A., Banks, H., Gregory, J.M., Johns, T.C., Mitchell, J.F.B., Wood, R.A., 2000. The simulation of SST, sea ice extents and ocean heat transports in a version of the Hadley Centre coupled model without flux adjustments. *Clim. Dyn.* 16 (2–3), 147–168.
- Greenwood, D.R., Archibald, S.B., Mathewes, R.W., Moss, P.T., 2005. Fossil biotas from the Okanagan Highlands, southern British Columbia and northeastern Washington State: climates and ecosystems across an Eocene landscape. *Can. J. Earth Sci.* 42 (2), 167–185.
- Greenwood, D.R., Wing, S.L., 1995. Eocene continental climates and latitudinal temperature gradients. *Geology* 23 (11), 1044–1048.
- Grein, M., Utescher, T., Wilde, V., Roth-Nebelsick, A., 2011. Reconstruction of the middle Eocene climate of Messel using palaeobotanical data. *Neues Jahrb. Geol. Paläontol. Abh.* 260 (3), 305–318.
- Hollis, C.J., Taylor, K.W.R., Handley, L., Pancost, R.D., Huber, M., Creech, J.B., Hines, B.R., Crouch, E.M., Morgans, H.E.G., Crampton, J.S., Gibbs, S., Pearson, P.N., Zachos, J.C., 2012. Early Paleogene temperature history of the Southwest Pacific Ocean: reconciling proxies and models. *Earth Planet. Sci. Lett.* 349–350 (0), 53–66.
- Hopmans, E.C., Schouten, S., Damsté, J.S.S., 2016. The effect of improved chromatography on GDGT-based palaeoproxies. *Org. Geochem.* 93, 1–6.
- Hopmans, E.C., Weijers, J.W., Schefuß, E., Herfort, L., Sinninghe Damsté, J.S., Schouten, S., 2004. A novel proxy for terrestrial organic matter in sediments based on branched and isoprenoid tetraether lipids. *Earth Planet. Sci. Lett.* 224 (1), 107–116.
- Huber, M., Caballero, R., 2011. The early Eocene equable climate problem revisited. *Clim. Past Discuss.* 7 (1), 241–304.
- Inagaki, F., Hinrichs, K.-U., Kubo, Y., Bowles, M.W., Heuer, V.B., Hong, W.-L., Hoshino, T., Ijiri, A., Imachi, H., Ito, M., 2015. Exploring deep microbial life in coal-bearing sediment down to ~2.5 km below the ocean floor. *Science* 349 (6246), 420–424.
- Inglis, G.N., Collinson, M.E., Riegel, W., Wilde, V., Robson, B.E., Lenz, O.K., Pancost, R.D., 2015a. Ecological and biogeochemical change in an early Paleogene peat-forming environment: linking biomarkers and palynology. *Palaeogeogr. Palaeoclimatol. Palaeoecol.* 438, 245–255.
- Inglis, G.N., Farnsworth, A., Lunt, D., Foster, G.L., Hollis, C.J., Pagan, M., Jardine, P.E., Pearson, P.N., Markwick, P., Galsworthy, A.M.J., Raynham, L., Taylor, K.W.R., Pancost, R.D., 2015b. Descent toward the icehouse: Eocene sea surface cooling inferred from GDGT distributions. *Paleoceanography* 30 (7), 1000–1020.
- Irvine, P.J., Gregoire, L.J., Lunt, D.J., Valdes, P.J., 2013. An efficient method to generate a perturbed parameter ensemble of a fully coupled AOGCM without flux-adjustment. *Geosci. Model Dev.* 6, 1447–1462. <http://dx.doi.org/10.5194/gmd-6-1447-2013>.
- Kiehl, J.T., Shields, C.A., 2013. Sensitivity of the Palaeocene–Eocene Thermal Maximum climate to cloud properties. *Philos. Trans. R. Soc. Lond. A, Math. Phys. Eng. Sci.* 371 (2001), 20130093.
- Lengger, S.K., Kraaij, M., Tjallingii, R., Baas, M., Stuut, J.-B., Hopmans, E.C., Sinninghe Damsté, J.S., Schouten, S., 2013. Differential degradation of intact polar and core glycerol dialkyl glycerol tetraether lipids upon post-depositional oxidation. *Org. Geochem.* 65 (0), 83–93.
- Lenz, O., Wilde, V., Mertz, D., Riegel, W., 2014. New palynology-based astronomical and revised  $^{40}\text{Ar}/^{39}\text{Ar}$  ages for the Eocene maar lake of Messel (Germany). *Int. J. Earth Sci.*, 1–17.
- Lunt, D.J., Dunkley Jones, T., Heinemann, M., Huber, M., LeGrande, A., Winguth, A., Loptson, C., Marotzke, J., Roberts, C.D., Tindall, J., Valdes, P., Winguth, C., 2012. A model–data comparison for a multi-model ensemble of early Eocene atmosphere–ocean simulations: EoMIP. *Clim. Past* 8 (5), 1717–1736.
- Lunt, D.J., Farnsworth, A., Loptson, C., Foster, G.L., Markwick, P., O'Brien, C.L., Pancost, R.D., Robson, S.A., Wrobel, N., 2016. Palaeogeographic controls on climate and proxy interpretation. *Clim. Past* 12 (5), 1181–1198.
- Naafs, D., Inglis, G., Zheng, Y., Amesbury, H., Biester, R., Bindler, R., Burrows, M.A., del Castillo Torres, D., Chambers, F.M., Cohen, A.D., Evershed, R.P., Feakins, S.J., Gallego-Sala, A., Gandois, L., Gray, D.M., Hatcher, P.M., Honorio Coronado, E.N., Hughes, P.D.M., Huguet, A., Kononen, M., Laggoun Defrage, F., Lahteenoja, O., Marchant, R., McClymont, E., Pontevedra Pombal, X., Ponton, C., Pourmand, A., Rizzuti, A.M., Schellekens, J., De Vleeschouwer, V., Pancost, R.D., in revision. Introducing global peat-specific temperature and pH calibrations based on brGDGT bacterial lipids. *Geoch. Cosmochim. Acta*.
- Pancost, R.D., Taylor, K.W., Inglis, G.N., Kennedy, E.M., Handley, L., Hollis, C.J., Crouch, E.M., Pross, J., Huber, M., Schouten, S., 2013. Early Paleogene evolution of terrestrial climate in the SW Pacific, Southern New Zealand. *Geochem. Geophys. Geosyst.* 14 (12), 5413–5429.
- Peterse, F., van der Meer, J., Schouten, S., Weijers, J.W.H., Fierer, N., Jackson, R.B., Kim, J.-H., Sinninghe Damsté, J.S., 2012. Revised calibration of the MBT–CBT paleotemperature proxy based on branched tetraether membrane lipids in surface soils. *Geochim. Cosmochim. Acta* 96 (0), 215–229.
- Pross, J., Contreras, L., Bijl, P.K., Greenwood, D.R., Bohaty, S.M., Schouten, S., Bendle, J.A., Röhl, U., Tauxe, L., Raine, J.J., 2012. Persistent near-tropical warmth on the Antarctic continent during the early Eocene epoch. *Nature* 488 (7409), 73–77.
- Riegel, W., Wilde, V., 2016. An early Eocene Sphagnum bog at Schöningen, northern Germany. *Int. J. Coal Geol.* 159, 57–70.
- Riegel, W., Wilde, V., Lenz, O.K., 2012. The Early Eocene of Schöningen (N-Germany) – an interim report. *Austrian J. Earth Sci.* 105/1, 88–109.
- Robson, B.E., Collinson, M.E., Riegel, W., Wilde, V., Scott, A.C., Pancost, R.D., 2015. Early Paleogene wildfires in peat-forming environments at Schöningen, Germany. *Palaeogeogr. Palaeoclimatol. Palaeoecol.* 437, 53–62.
- Sagoo, N., Valdes, P., Flecker, R., Gregoire, L.J., 2013. The Early Eocene equable climate problem: can perturbations of climate model parameters identify possible solutions? *Philos. Trans. R. Soc. A, Math. Phys. Eng. Sci.* 371 (2001).
- Schouten, S., Hopmans, E.C., Sinninghe Damsté, J.S., 2013. The organic geochemistry of glycerol dialkyl glycerol tetraether lipids: a review. *Org. Geochem.* 54, 19–61.
- Sinninghe Damsté, J.S., Ossebaar, J., Schouten, S., Verschuren, D., 2012. Distribution of tetraether lipids in the 25-ka sedimentary record of Lake Challa: extracting reliable TEX<sub>86</sub> and MBT/CBT palaeotemperatures from an equatorial African lake. *Quat. Sci. Rev.* 50, 43–54.
- Snell, K.E., Thrasher, B.L., Eiler, J.M., Koch, P.L., Sloan, L.C., Tabor, N.J., 2013. Hot summers in the Bighorn Basin during the early Paleogene. *Geology* 41 (1), 55–58.
- Standke, G., 2008. Paläogeografie des älteren Tertiärs (Paleozän bis Untermyozän) im mitteldeutschen Raum. *Zeitschrift der deutschen Gesellschaft für Geowissenschaften* 159 (1), 81–103.
- Weber, Y., De Jonge, C., Rijpstra, W.I.C., Hopmans, E.C., Stadnitskaia, A., Schubert, C.J., Lehmann, M.F., Damsté, J.S.S., Niemann, H., 2015. Identification and carbon isotope composition of a novel branched GDGT isomer in lake sediments: evidence for lacustrine branched GDGT production. *Geochim. Cosmochim. Acta* 154 (0), 118–129.
- Weijers, J.W., Schouten, S., van den Donker, J.C., Hopmans, E.C., Sinninghe Damsté, J.S., 2007. Environmental controls on bacterial tetraether membrane lipid distribution in soils. *Geochim. Cosmochim. Acta* 71 (3), 703–713.
- Weijers, J.W.H., Schefuß, E., Kim, J.-H., Sinninghe Damsté, J.S., Schouten, S., 2014. Constraints on the sources of branched tetraether membrane lipids in distal marine sediments. *Org. Geochem.* 72 (0), 14–22.
- Weijers, J.W.H., Steinmann, P., Hopmans, E.C., Schouten, S., Sinninghe Damsté, J.S., 2011. Bacterial tetraether membrane lipids in peat and coal: testing the MBT–CBT temperature proxy for climate reconstruction. *Org. Geochem.* 42 (5), 477–486.
- Wilf, P., 2000. Late Paleocene–early Eocene climate changes in southwestern Wyoming: paleobotanical analysis. *Geol. Soc. Am. Bull.* 112 (2), 292–307.

- Zachos, J., Pagani, M., Sloan, L., Thomas, E., Billups, K., 2001. Trends, rhythms, and aberrations in global climate 65 Ma to present. *Science* 292 (5517), 686–693.
- Zell, C., Kim, J.H., Balsinha, M., Dorhout, D., Fernandes, C., Baas, M., Sinninghe Damsté, J.S., 2014. Transport of branched tetraether lipids from the Tagus River basin to the coastal ocean of the Portuguese margin: consequences for the interpretation of the MBT/CBT paleothermometer. *Biogeosci. Discuss.* 11 (3), 3731–3776.
- Zheng, Y.H., Li, Q.Y., Wang, Z.Z., Naafs, B.D.A., Yu, X.F., Pancost, R.D., 2015. Peatland GDGT records of Holocene climatic and biogeochemical responses to the Asian Monsoon. *Org. Geochem.* 87, 86–95.